



## Phytofabrication of Selenium Nanoparticles for Investigating Their Efficacy as Nanotherapeutics Against Lung Carcinoma Cells and Bacterial Pathogens

P. CHRISTINA RUBY STELLA, A. ANGEL PRABA\* and A. NIVETHA

Department of Chemistry, Holy Cross College (Autonomous), Affiliated to Bharathidasan University, Palkalaiperur, Tiruchirappalli, India.

\*Corresponding author E-mail: angelpraba98@gmail.com

<http://dx.doi.org/10.13005/ojc/410127>

(Received: August 30, 2024; Accepted: January 10, 2025)

### ABSTRACT

The synthesis of nanoparticles has garnered significant interest due to their unique properties and broad potential applications. This study explores the synthesis of selenium nanoparticles (Se NPs) using *Justicia adhatoda* leaf extract and evaluates their anti-lung cancer activity on A549 cells. The leaf extract was characterized through preliminary phytochemical screening and GC-MS analysis, which identified bioactive compounds with potential therapeutic effects. The synthesized Se NPs were characterized by UV-Visible spectroscopy, revealing a maximum absorbance at 204 nm, and FT-IR spectroscopy, which confirmed the presence of elemental selenium at 617 cm<sup>-1</sup>. XRD analysis indicated an FCC structure and spherical morphology with a crystallite size of 43 nm. SEM and TEM imaging confirmed a spherical shape, with an average nanoparticle size of 5 nm. Thermal analysis showed a degradation temperature of 497°C, suggesting thermal stability. Biological assessments demonstrated that Se NPs exhibited stronger antimicrobial activity against *Staphylococcus aureus* compared to *Escherichia coli*, high cell viability (88%) in PBMC cells at 10 µg/mL, significant cytotoxicity (81%) against A549 lung cancer cells at 500 µg/mL, and potent anti-inflammatory activity through the inhibition of IL-6 cytokine production. These findings underscore the promising physicochemical and biological properties of Se NPs, indicating their potential as therapeutic agents for anti-lung cancer and anti-inflammatory treatments. Further investigation is necessary to fully evaluate their therapeutic potential.

**Keywords:** Phytochemicals, COPD, GC-MS, XRD, Cytotoxicity.

### INTRODUCTION

#### COPD and the Potential of *J. adhatoda*-Derived Selenium Nanoparticles

Chronic Obstructive Pulmonary Disease (COPD) is a life-threatening condition primarily caused by air pollution and exposure to harmful

chemicals in tobacco smoke. Key symptoms include phlegm-clogged lungs, wheezing, persistent coughing, and difficulty breathing due to airway inflammation and obstruction.<sup>1</sup> Over time, COPD can lead to severe complications, including pneumonia, asthma, chronic bronchitis, lung cancer, and heart diseases.<sup>2</sup>



For centuries, herbal medicines have been integral to disease management due to their bioactive compounds. Among them, *Justicia adhatoda* (commonly known as Vasaka or Malabar nut) is a medicinal shrub widely found in Asia. Its leaves are rich in flavonoids, alkaloids, tannins, saponins, and phenolics, contributing to its therapeutic properties.<sup>4</sup> Traditionally, *J. adhatoda* has been utilized to treat respiratory ailments such as cough, bronchitis, colds, asthma, and tuberculosis.<sup>3</sup>

### Nanotechnology and Selenium Nanoparticles

Nanotechnology has transformed the pharmaceutical landscape, introducing innovative drug delivery systems and enhancing therapeutic efficacy. Selenium nanoparticles (SeNPs), synthesized through physical, chemical, or biological methods, have emerged as a promising tool in biomedical research. Green synthesis of SeNPs, particularly using plant extracts, is notable for its high biocompatibility and eco-friendliness.<sup>5</sup>

### Therapeutic Applications of Selenium Nanoparticles

Selenium nanoparticles possess remarkable therapeutic properties, including anti-inflammatory, anti-parasitic, and anti-cancer activities.<sup>7</sup> Their nanoscale structure facilitates interaction with bacterial cells, inhibiting attachment and growth. Selenium is an essential micronutrient, vital for the functioning of enzymes and proteins that protect against oxidative stress and cellular damage. A selenium deficiency can result in neurological disorders, cardiovascular issues, and weakened immunity.

Nano-selenium exhibits a range of bioactivities, including anti-cancer, anti-inflammatory, and anti-diabetic effects.<sup>8,9,10</sup> This study synthesized selenium nanoparticles using aqueous leaf extracts of *J. adhatoda* and evaluated their efficacy against inflammatory cytokines implicated in COPD, lung cancer, and bronchitis. In this study, we utilized the Soxhlet extraction method to obtain bioactive compounds from *J. adhatoda* leaves. For the synthesis of selenium nanoparticles (Se NPs), we employed the decoction method, using ascorbic acid as a natural reducing agent. Ascorbic acid facilitates the reduction of selenium ions to nanoscale selenium particles, ensuring eco-friendly and efficient nanoparticle synthesis. The combination of phytochemicals from *J. adhatoda* and the antioxidant

properties of ascorbic acid enhances the therapeutic potential of the synthesized Se NPs.

## MATERIALS AND METHODS

### Chemicals used

The following chemicals and materials were utilized in the study:

Sodium selenite and ascorbic acid essential for the synthesis of selenium nanoparticles, were procured from Sigma Aldrich, India. Double-distilled water was prepared in-house for all experimental procedures to ensure purity. Muslin cloth and Whatman No. 1 filter paper were purchased from Precision Scientific Co., Tamil Nadu, India, and were used for filtration during extraction and synthesis processes. These high-quality reagents and materials contributed to the reliability and reproducibility of the synthesis and characterization of selenium nanoparticles.

### Botanical Sample Acquisition

*J. adhatoda* leaves were collected from Ariyalur, Tamil Nadu, India. To ensure cleanliness, the leaves were washed thoroughly with tap water to remove dust and other impurities. The washed leaves were dried in the shade at room temperature for 15 days to retain their phytochemical properties. After drying, a mechanical blender was used to grind the leaves into a fine powder, which was stored in an airtight container for subsequent extraction and synthesis procedures.



Fig. 1. Collection of Plant Samples

### Extraction of Leaf Biomolecules

Approximately 60 g of finely powdered *J. adhatoda* leaves was placed in a thimble of a Soxhlet apparatus. A round-bottom flask containing 250 mL of double-distilled water served as the solvent. The Soxhlet apparatus was heated using a heating mantle set to a temperature range of 60°C to 80°C, and the extraction process was conducted for 6 hours. The extract obtained was evaporated to

dryness under controlled temperature and pressure conditions. The dried extract was then stored in an airtight container at 4°C for further use.

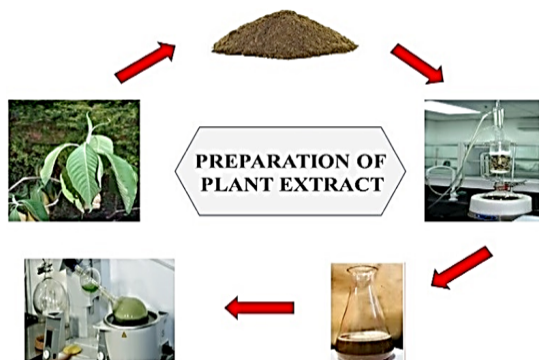


Fig. 2. Preparation of plant extract

### Biogenic production of selenium nanoparticles For nanoparticle synthesis

100 mL of a 2 g concentrated plant extract was diluted with double-distilled water. 100 mL of a 20 mM ascorbic acid solution was prepared in a

standard flask. 100 mL of a 40 mM aqueous sodium selenite solution was also prepared.

Plant extract, sodium selenite solution, and ascorbic acid were mixed in varying ratios (9:1, 8:2, 7:3, 6:4, and 5:5) and incubated for 24 hours. Among these, the 5:5 ratio demonstrated the highest nanoparticle yield and was chosen for bulk preparation.

### Bulk Preparation

50 mL each of the plant extract, sodium selenite solution, and ascorbic acid were mixed and stirred at 90°C and 1200 rpm for 45 minutes. The formation of selenium nanoparticles was visually confirmed by the appearance of a red colour in the reaction mixture. The reaction mixture was incubated for 24 h and centrifuged to separate the nanoparticles. The residue obtained was dried in a microwave oven at 250°C and subsequently calcinated. The final product was stored for further characterization and pharmacological evaluations.

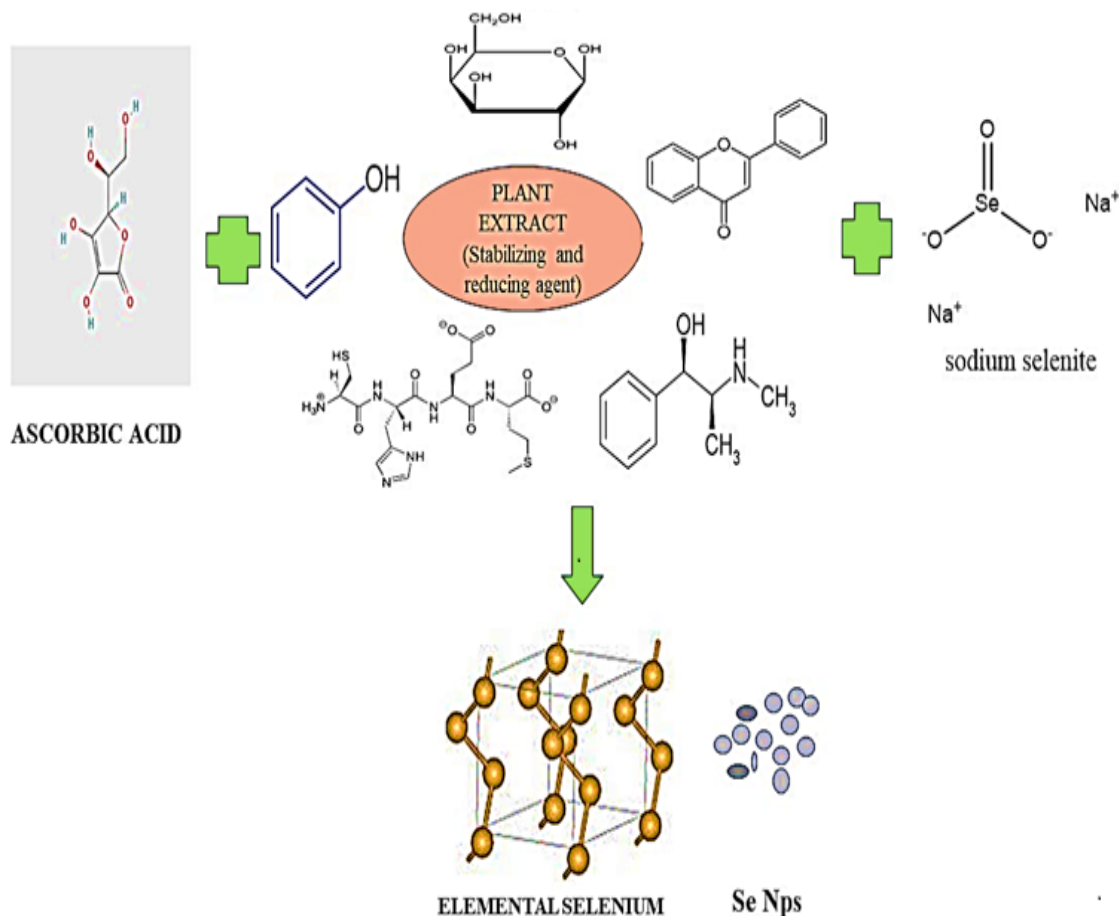


Fig. 3. Mechanism of sodium selenite reduction into selenium nanoparticles

### Physicochemical analysis of leaf extract

#### Comprehensive qualitative assessment

The main classes of phytochemicals present in plant extract were revealed by qualitative analysis. Froth test,  $\text{FeCl}_3$  test, Wagner test, Alkaline reagent test, Flame test, Molisch test, Lead acetate test, Mayers test and further screening tests were used for the identification of bio-active compounds, which are necessary for discovering the natural therapeutic agents.

#### GC-MS

The mass spectrum revealed the molecular formula, mass spectrum, and molecular structure of secondary metabolites present in plant extract. The retention time of identified phytochemicals with known standards was also determined. GC-MS analysis for leaf extract was analysed from Shimadzu-QP2020 which has a wide practical mass range region from 1.5 to 1090m/z. A gas chromatogram helps in the separation of volatile compounds present in the sample whereas the mass spectrum helps in the identification of the component's fragment based on their mass.

### Morphological and structural characterization of selenium nanoparticles

#### Analytical Instrumentation Techniques

A suite of analytical techniques was employed to characterize the synthesized selenium nanoparticles (SeNPs)

#### UV-Visible Spectroscopy

UV-Visible spectroscopy was used to analyze the optical properties of nanoparticles. The plant extract showed a wavelength range between 200-800 nm, while the synthesized nanoparticles were measured using a Perkin-Elmer UV-Visible spectrometer ( $\lambda_{35}$ ) with a range of 190-1100 nm. Excited electrons caused distinct peaks, with higher absorbance and greater wavelengths corresponding to easier electron transitions.

#### FT-IR Analysis

FT-IR spectra were recorded using a Perkin-Elmer spectrometer with a spectral range of  $450\text{ cm}^{-1}$  to  $4000\text{ cm}^{-1}$ . IR absorption peaks were used to determine molecular structures and band vibrations of the synthesized nanoparticles.

### XRD Analysis

X-ray diffraction (XRD) was performed using an HTK1200N-Bruker D8 with copper as the anode material and an accuracy of  $\pm 0.0025$  degrees. The analysis provided data on the chemical composition, lattice strains, and texture of the nanoparticles. The size of nanocrystals was calculated using the Debye-Scherrer equation  $D = K\lambda/\beta\cos\theta$

where:

D= Crystallite size of nanoparticles

K=Scherrer constant (0.98)

$\lambda$ =Wavelength (1.54 Å)

B= Full width at half maximum (FWHM)

$\theta$ =Position ( $2\theta$  in degrees)

### SEM and TEM Imaging

Scanning Electron Microscopy (SEM) provided morphological details of nanoparticles by detecting reflected electrons from the surface. Images were obtained at magnifications ranging from 2.94x to 40.00x with a high-tension value of 10.00 kV. Transmission Electron Microscopy (TEM) captured nanoscale details at various magnifications under an accelerating voltage of 20 kV.

### EDX Analysis

Energy Dispersive X-ray (EDX) analysis confirmed the purity of the nanoparticles, with an optical absorption peak observed at 3 keV.

### TGA and DSC Analysis

Thermogravimetric Analysis (TGA) and Differential Scanning Calorimetry (DSC) were performed to study thermal stability and decomposition. TGA was conducted using a Mettler Toledo thermogravimeter (TG2), analyzing approximately 3 g of the sample up to  $600^\circ\text{C}$  under controlled conditions.

### Anti-microbial efficacy

The antibacterial activity of selenium nanoparticles was tested against *Staphylococcus aureus* and *Escherichia coli*. These bacterial strains were acquired from MTCC, Chandigarh, India.

### Methodology

The disc diffusion method was employed. 10 mL of agar medium was poured into sterile Petri dishes and inoculated with test organisms.

Sample-loaded discs at varying concentrations were placed on the agar. Amoxicillin (5 µg) served as the positive control.

### Incubation and Observation

Plates were incubated at room temperature for 24 h, and the inhibition zones were measured to assess antibacterial efficacy.

### MTT assay for assessing cellular metabolic activity

To evaluate cytotoxicity, an MTT assay was performed using PBMC and A549 cell lines.

### Cell Preparation

PBMC cells were cultured in RPMI medium with 10% FBS and 1% antibiotic solution, maintained at 37°C with 5% CO<sub>2</sub>. Under identical conditions, A549 cells were cultivated in DMEM medium.

### Procedure

Cells were seeded at a density of  $1 \times 10^5$   $\times$   $10^5$  cells/mL in 200 µL of medium per well in a tissue culture plate. After incubation, 10 µL of 5 mg/mL MTT solution was added to each well, forming formazan crystals.

### Inhibition of inflammatory responses and mediators

The anti-inflammatory activity of selenium nanoparticles was evaluated by measuring IL-6 cytokine levels using sandwich ELISA. Lipopolysaccharide (LPS) was used to induce inflammation and trigger cytokine production. Synthesized nanoparticles were tested for their ability to inhibit IL-6 cytokine levels. Inhibition concentrations were quantified at 450 nm.

### Observations and analysis

#### Comprehensive qualitative assessment

Aqueous leaf extract was subjected to phytochemical screening. Screening test confirms the appearance of bioactive components like alkaloids, saponin, flavonoids, tannin, proteins, terpenoids, and glycosides and the absence of phytochemicals such as steroids, carbohydrates, reducing sugars and amino acids in aqueous plant extract whereas Methanol plant extract showed the presence of Terpenoids, Alkaloids, Flavonoids, Tannin, Xanthoprotein, Saponin, Steroids, Coumarins and cardiac glycosides and absence of carbohydrate, amino acids, phenol and reducing sugars. In the

present study, these bio-active compounds help in the treatment of COPD, and the phytochemicals are responsible for anti-inflammatory, cytotoxicity, and anti-bacterial activity.

**Table 1: Screening of Aqueous Plant Extract**

Phytochemicals	Aqueous extract
Alkaloids	+++
Flavonoids	+++
Saponin	++
Tannin	+++
Terpenoids	++
Steroids	-
Phenol	+
Amino acids	-
Carbohydrates	-
Xanthoproteins	+
Coumarins	-
Reducing sugar	++
Cardiac glycosides	+

(+=slightly present, ++=moderately present, +++=strongly present)

### GC-MS

Compounds with low molecular weight were detected by GC-MS. The mass range of GC-MS is 30-400 m/z for lower molecular weight molecules and 30-600 m/z for greater molecular weight molecules (which has a wide spectrum). The temperature for the measurement was set between 300 and 600°C. GC-MS helps in the identification of bioactive compounds and their higher sensitivity through gas chromatograms. The aqueous leaf extract showed 20 compounds in GC-MS analysis. 2-alpha-bromo-4-alpha-phthalimido bicyclo [3.2.1] oct-6-en-3-one showed a height% of 25.9 with 34.858 retention time, 4-methyl-1H-pyranolo[4,3-c] pyridine, 1H-furo[3,4-c] pyrrole-4-carboxylic acid are the alkaloid derivatives with the retention time of 38.181, 39.28, and 39.622 respectively whereas 3,4-dihydroxyphenylglycol, 4TMS derivative, Ethane diamide, n, n'-bis[2-[(3,5-dimethoxy phenyl) amino] oxo acetyl]phenyl]-, are the phenolic compounds with retention time of 38.893 and 39.32. 6-(2-furanyl) hexahydro-1,3-dioxo-4-phenyl is the terpenoid derivative with a 39.28 retention time.

### UV

Nanoparticles possess unique optical and spectral properties, including distinct absorbance characteristics. The UV-Vis spectrum was employed to identify and confirm the formation of selenium nanoparticles. The spectrum of the synthesized

nanoparticles was analyzed over a range of 200 nm to 1200 nm. Selenium nanoparticles were reduced from selenite ions, as confirmed by the absorption spectrum obtained between 200 nm and 400 nm. A strong absorption peak at 204 nm in the UV region confirmed the presence of selenium nanoparticles synthesized from aqueous plant extract. The strong absorbance observed was attributed to the concentration of the sample, indicating the crystalline nature of the synthesized nanoparticles.

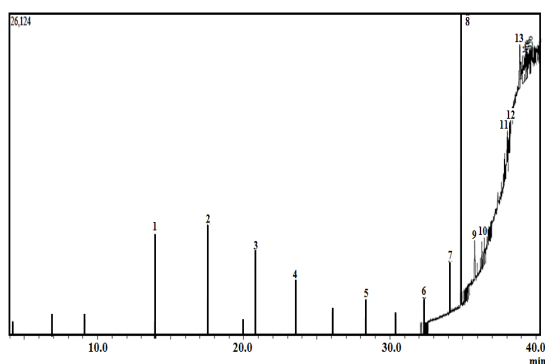


Fig. 4. Gas Chromatogram of Plant Extract

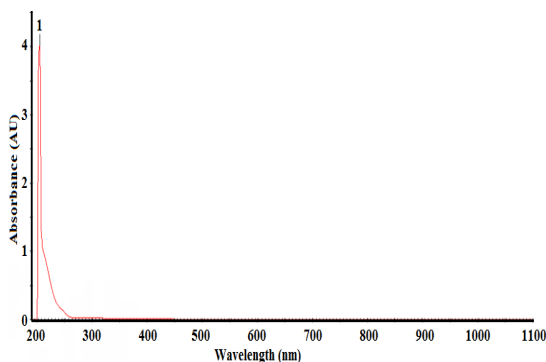


Fig. 5. UV Spectrum of se nanoparticles

#### FT-IR

Symmetric and asymmetric stretching bending vibrational frequencies of the molecular structure were monitored and characterized by FT-IR. Adsorbed biomolecule conjugation and nanomaterials conjugation were identified from spectral bands of the FT-IR technique. The nature of materials and bond atoms in aqueous nanoparticles were indicated by the peak intensities and vibrational frequencies of the FT-IR spectrum. In given spectrum, the broad intense peak at  $3435.82\text{ cm}^{-1}$  was due to the hydroxyl group (-O-H- stretching). The strong absorption band at  $2026.31\text{ cm}^{-1}$  and  $2076.45\text{ cm}^{-1}$  shows the presence of iso thiocyanate. The band at  $1638.04\text{ cm}^{-1}$  is due to the stretching

vibrations of -C=C- conjugated alkene. Bending vibrations at  $1384.42\text{ cm}^{-1}$  belong to the -C-H group of alkane or aldehyde. The band at  $1269.34\text{ cm}^{-1}$  corresponds to the -C-O- stretch of aromatic esters whereas  $1120.96\text{ cm}^{-1}$  shows the presence of the sulfonic acid group (-S=O). The broad absorption spectrum at  $991.62\text{ cm}^{-1}$  corresponds to the bending vibrations of mono-substituted alkene (-C=C-). The broad intense band in the fingerprint region at  $617\text{ cm}^{-1}$  corresponds the stretching vibrations of elemental selenium.

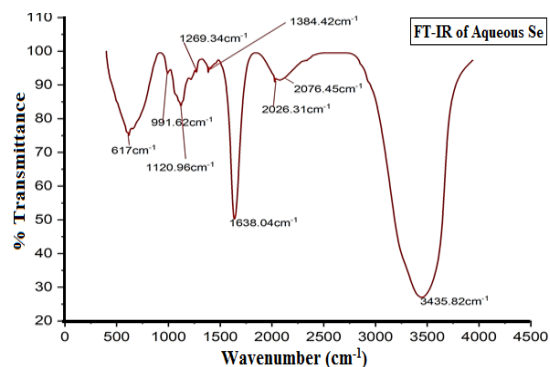


Fig. 6. FT-IR Spectra of se nanoparticles

#### XRD

The crystalline structure of synthesized selenium nanoparticles was illustrated by comparing the intensities and peak positions of known crystals. Synthesized nanoparticles were reduced from 2 $\theta$  values corresponding to crystal planes (hkl values). According to Miller's indices of XRD, the crystal structure of selenium is spherical shaped. Sharp diffraction peaks confirm the crystalline nature of selenium nanoparticles. Higher intensity peak gives the diffraction pattern of nanoparticles which are responsible for crystalline structure. The sharp peaks at  $28.43^\circ$ ,  $30.98^\circ$ ,  $37.39^\circ$ ,  $55.68^\circ$ , and  $58.39^\circ$  show corresponding crystal planes (111), (200), (220), (311), (220) which confirms the crystalline nature of selenium. The high intense peak at  $28^\circ$  corresponds to the 111-diffraction plane showing the FCC phase of selenium. The intensity of peaks describes the crystallinity of nanoparticles.

#### TGA

The decomposition process in the first step occurred between  $32$  and  $161^\circ\text{C}$ , which was due to moisture evaporation that adsorbed on the surface of selenium nanoparticles. Weight loss was noted for about 0.9%. In the second step, further heating of the sample leads to an oxidation process and a sudden change in mass. The third step shows the

degradation of the sample between 497 and 595 with a weight loss of about 0.5% attributed to organic compound decomposition (such as reducing sugar) which was a stabilizing agent. Thus, TGA confirmed that the synthesized nanoparticle was thermally stable and resistant to heat and can be used for bio-medical purposes.

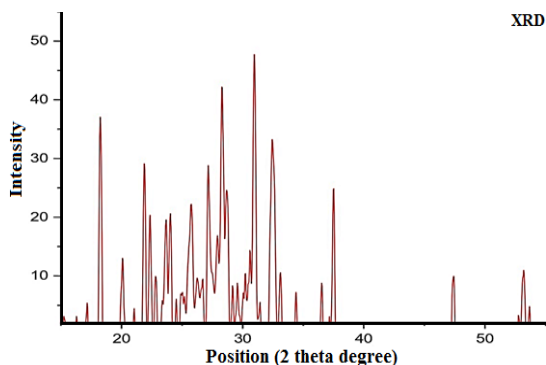


Fig. 7. XRD Spectrum of se nanoparticle

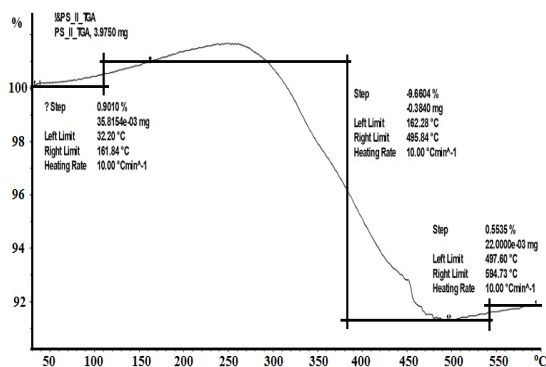


Fig. 8. TGA of selenium nanoparticles

**Morphological structure of synthesized selenium nanoparticles**

Morphological investigation of synthesized nanoparticles was illustrated using SEM and TEM images. The size distribution and shape of selenium nanoparticles were revealed by SEM analysis which scans the surface of the nanoparticles and produces the image of the sample whereas TEM creates an image by transmitting the electrons through the nanoparticles. At an accelerating voltage of 20 and 200kv, SEM and TEM images confirmed that the shape of synthesized selenium nanoparticles was spherical. TEM image confirmed the single crystal size of the nanoparticles at 5 nm. The reduced selenium nanoparticles were subjected to EDX analysis in order to know the purity and chemical composition. EDX showed the weight % of elements such as selenium and oxygen were 52.12% and 47.88% respectively. Thus, EDX

proves that the synthesized nanoparticles were selenium.

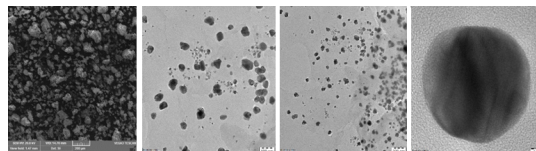


Fig. 9. SEM and TEM of Selenium Nanoparticles

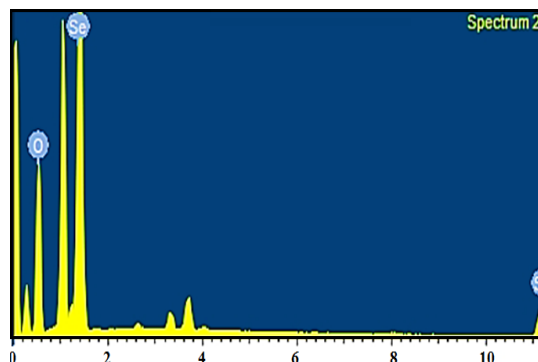


Fig. 10. EDX of capped selenium nanoparticles

**Therapeutic effects and biological activities**  
**Inhibition of bacterial growth and biofilm formation**

*S. aureus* and *E. coli* were the pathogenic bacterial strains tested against greenly synthesized selenium nanoparticles. Amoxicillin drug was used as a standard for this activity. The concentration of standard amoxicillin was 10 µL/disc which showed the inhibition rate for *E. coli* and *S. aureus* as 10mm and 8mm respectively. Synthesized selenium nanoparticles were taken under different concentrations such as 60 µg/mL, 80 µg/mL, and 100 µg/mL. As the concentration of sample increases, the inhibition rate of bacterial strains also as shown in Table. MIC of *S. aureus* increases from 3mm to 6mm and MIC for *E. coli* increases from 1mm to 3mm respectively. MIC is greater for *S. aureus* than *E. coli*. Thus, greenly synthesized selenium nanoparticles act as an efficient anti-bacterial agent.

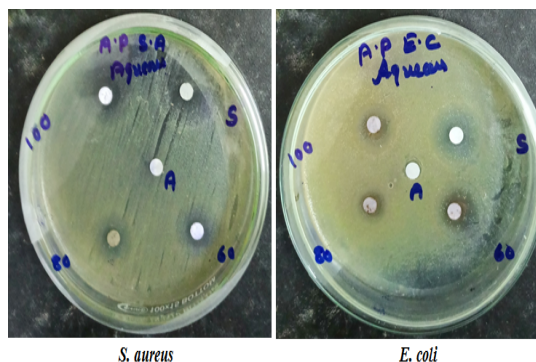


Fig. 11. Antimicrobial Efficacy Against Bacterial Pathogens

**Table 2: Inhibition rate of microbials against selenium nanoparticles**

Samples	Concentration (µL/mL)	Organisms/Zone of inhibition (mm)	
		<i>S. aureus</i>	<i>E. coli</i>
AS-I	60	3	1
AS-II	80	4	2
AS-III	100	6	3
Standard Amoxicillin	10 µL	10	8
DD WATER	10 µL	0	0

**MTT-based cytotoxicity and cell proliferation analysis**

PBMC cells are immune cells that protect our body from diseases and act as defense cell lines from diseases and infections. Synthesized selenium nanoparticles were tested against PBMC cells in order to know the cell viability. As the concentration of the sample decreases, the viability of cells increases. The potency of the drug is determined by the IC<sub>50</sub> concentration of the sample. Thus, the IC<sub>50</sub> of the tested sample is said to be 112.4 mg/mL. It shows that synthesized nanoparticles are non-toxic for PBMC cells. Graphical representation shows the cytotoxicity and cell viability of immune (PBMC) cells.

**Table 3: Analysis of Apoptosis and Cell Death in PBMCs**

Sr. No	Sample conc. in (µg/mL)	Cell viability(%)
1	Control	100
2	500	50.948383
3	400	52.188771
4	300	57.090774
5	200	63.423333
6	100	75.358034
7	80	78.104228
8	60	81.440421
9	40	85.053734
10	20	86.505712
11	10	88.98782

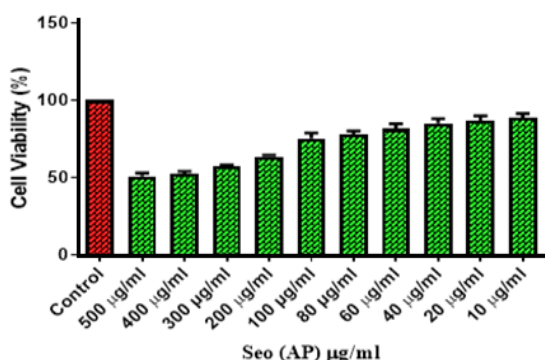
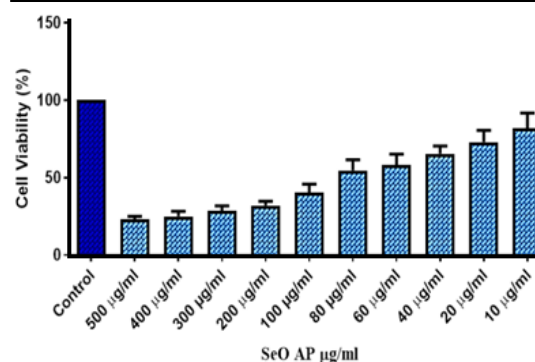


**Table 4: Toxicity Assessment of A549 Cells**

Sr. No	Sample conc. in (µg/mL)	Cytotoxicity(%)
1	Control	100
2	10	81.983207
3	20	72.986759
4	40	65.510235
5	60	72.986759
6	80	54.726549
7	100	40.522358
8	200	32.022618
9	300	28.66029
10	400	25.11327
11	500	23.23707



On the other hand, selenium nanoparticles were tested against A549 cells to know the potential of the drug. As concentration increases, the cytotoxicity of cells also increases. Cell viability of A549 cells decreases from 81.98 to 23.30 µg/mL as mentioned in Table 4. The amount of drug needed for the inhibition of A549 cells was 56.36 µg/mL. As the potential of the drug is greater, selenium nanoparticle acts as an efficient anti-cancer drug.

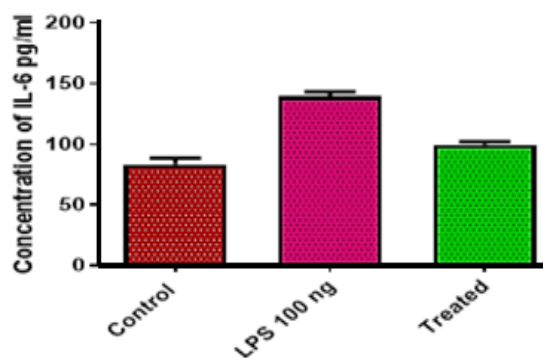
**Inhibition of inflammatory responses and mediators**

**ELISA**

The initial concentration of IL-6 cytokine was 83.376 pg/mL. After inducing the inflammation with Lipopolysaccharide (LPS), the inflammatory concentration was increased to 139.490 pg/mL. The induced IL-6 was treated against synthesized selenium nanoparticles and the concentration was noted which was reduced to 99.738 pg/mL respectively. ELISA test confirms that selenium nanoparticles exhibit effective potential against inflammatory cytokines and act as the best anti-inflammatory agent. The inhibitory concentration of IL-6 cytokine is shown in the Table 5.

**Table 5: Evaluation of inflammatory responses**

Sr. No	Name	Concentration of IL-6 (pg/mL)
1	Control	83.376
2	LPS	139.490
3	Treated	99.738



### CONCLUSION

ELISA confirms that selenium nanoparticles have the potential for inflammatory cytokine. MTT Assay explains that nanoparticles have the best potency for drugs as PBMC cells have the IC<sub>50</sub> concentration of 112.4 mg/mL. Thus, this study concludes that synthesized nanoparticles are

harmless to immune cells (PBMC). The qualitative analysis explained the presence and absence of bioactive compounds in aqueous leaf extract. GC-MS technique illustrated the secondary metabolites present in leaf extract along with its molecular formula and mass spectrum. UV confirmed the formation of selenium nanoparticles at 204nm, whereas FT-IR shows the maximum binding groups of selenium nanoparticles. XRD explains the crystal size, structure, and lattice planes of the nanoparticles whereas SEM and TEM confirm the morphological structure of synthesized selenium nanoparticles. TGA illustrates the thermal stability by melting point and weight loss of nanoparticles whereas DSC shows the glass transition and endothermic behaviour of nanoparticles.

### ACKNOWLEDGEMENT

Acknowledgement is made to the Chemistry Research Department, Holy Cross College, Tiruchirappalli, for provision of laboratory facilities and technical support.

### Conflict of interest

Authors declare no conflicts of interest.

### REFERENCES

- Vestbo, J.; Hurd, S. S.; Agustí, A. G.; Jones, P.W.; Vogelmeier, C.; Anzueto, A., *European Respiratory Journal.*, **2013**, 43(3), 1-22.
- Barnes, P. J., *The New England Journal of Medicine.*, **2000**, 343(4), 269-280.
- Dey, S. K.; Thakur, J.S.; Gupta, P.C.; Swaminathan, R., *International Journal of Green Pharmacy.*, **2018**, 12(4), 302-310.
- Thakur, M.; Kunwar, R.M.; Paudel, H.R.; Bhatta, S.; Joshi, L.R., *Journal of Ethnopharmacology.*, **2016**, 194, 426-434.
- Huang, Y.; Chen, Q.; Zeng, H.; Yang, C., *Frontiers in Pharmacology.*, **2016**, 7, 1-12.
- Hussain, I.; Lakhan, M.N.; Hanan. A.; Soomro, I.A., *Journal of Nanoscience and Nanotechnology.*, **2020**, 20(10), 6162-6177.
- Li, Y.; Lin, W.; Zhang, J.; Fa xu, J., *International J. of Nanomedicine.*, **2020**, 15, 2809-2822.
- Husen, A.; Siddiqi, K. S., *Journal of Nanobiotechnology.*, **2014**, 12, 28.
- Fardsadegh, B.; Malmiri, J. H., *Green Process. Synth.*, **2019**, 8, 399-407.
- Tomotake, H.; Koga, T.; Yamato, M.; Kassu, A.; Ota, F., *J. Nutri. Sci. Vitaminol.*, **2006**, 52, 157-160
- Ramamurthy, C. H.; Sampath, K. S.; Arunkumar, P.; Suresh kumar, M.; Sujatha, V.; Premkumar, K.; Thirunavukkarasu, C., *Bioprocess and Biosystems Engineering.*, **2013**, 36(8), 1131-1139.
- Alagesan, V.; Venugopal, S., *Bio.Nano. Science.*, **2019**, 9, 105-116.
- Arokiyaraj, S.; Vincent, S.; Saravanan, M.; Lee, Y.; Oh, Y.K.; Kim, K.H., *Nanomedicine and Biotechnology.*, **2017**, 45, 372-379.
- Chaudhary, S.; Umar, A.; Mehta, S.K., *Progress in Materi. Sci.*, **2016**, 83, 270-329.
- Hosnedlova, B.; Kepinska, M.; Skalickova, S., *Interna. J. of Nanomedi.*, **2018**, 13, 2107-2128.
- Dhanjal, S.; Cameotra, S., *Microb Cell Fact.*, **2010**, 9, 1-11.
- Reddy, V.; Torati, RS.; Oh, S.; Kim, C., *Ind Eng Chem Res.*, **2012**, 52, 556-564.
- Bharathi, S.; Kumaran, S.; Suresh, G.; Ramesh, M.; Thangamani, V.; Pugazhvendan, S.; Sathiyamurthy, K., *Biocatal. Agric. Biotechnol.*, **2020**, 27, 101655.
- Chen, H.; Yoo, J.B.; Liu, Y.; Zhao, G., *Electron. Mater. Lett.*, **2011**, 7(4), 333-336.
- Cittrarasu, V.; Balasubramanian, B.; Kaliannan, D.; Park, S.; Maluventhan, V.; Kaul, T.; Liu, W.C.; Arumugam, M. *Artif., Cells. Nanomed. Biotechnol.*, **2019**, 47(1), 2424-2430.